

# Approximate Bayesian inference for joint partially linear modeling of longitudinal measurements and spatial time-to-event data

T. Baghfalaki<sup>\*,1</sup>, M. Ganjali<sup>2</sup> and R. Martins<sup>3</sup>

<sup>1</sup>Department of Mathematics, The University of Manchester, Manchester, UK

<sup>2</sup>Department of Statistics, Faculty of Mathematical Sciences, Shahid Beheshti University, Tehran, Iran.

<sup>3</sup>Faculdade de Ciências da Universidade de Lisboa (FCUL), Centro de Estatística e Aplicações da Universidade de Lisboa (CEAUL), Lisboa, Portugal.

## Abstract

The integration of longitudinal measurements and survival time in statistical modeling offers a powerful framework for capturing the interplay between these two essential outcomes, particularly when they exhibit associations. However, in scenarios where spatial dependencies among entities are present due to geographic regions, traditional approaches may fall short. In response, this paper introduces a novel approximate Bayesian hierarchical model tailored for jointly analyzing longitudinal and spatial survival outcomes. The model leverages a conditional autoregressive structure to incorporate spatial effects, while simultaneously employing a joint partially linear model to capture the nonlinear influence of time on longitudinal responses. Through extensive simulation studies, the efficacy of the proposed method is rigorously evaluated. Furthermore, its practical utility is demonstrated through an application to real-world HIV/AIDS data sourced from various Brazilian states, showcasing its adaptability and relevance in epidemiological research.

Keywords: Approximate Bayesian inference; Integrated Laplace approximation (INLA); Joint modeling; Latent Gaussian model; Spatial effects; Spline functions.

## 1 Introduction

In numerous clinical longitudinal studies, data on longitudinal markers are gathered until an event occurs [44, 18]. For instance, in HIV studies, CD4 counts are typically monitored until a patient's demise or dropout from the study, highlighting the interplay between longitudinal and survival processes. However, these processes are often analyzed separately, leading to biased parameter estimates [26]. The solution lies in joint modeling, a burgeoning field with extensive medical applications [12, 56, 35, 13, 22, 57].

Joint modeling typically involves two submodels: the longitudinal submodel, often a linear mixed effects model [62], and the survival submodel, ranging from the traditional Cox model to accelerated failure time models [33]. Central to joint modeling is the establishment of a linking structure, often achieved by sharing random effects between the longitudinal and survival processes [44, 18].

Recent years have seen significant advancements in research within this domain, extending beyond the conventional framework to analyze diverse data scales such as counts or ordinal longitudinal outcomes [34, 2, 5, 64, 3], as well as multivariate longitudinal outcomes [14, 4, 36, 29, 32]. Additional extensions include addressing competing risks, multiple causes of death [60, 34, 30, 55, 5], and cure fraction models [11, 63]. For a comprehensive review of joint modeling, readers may refer to [53, 43, 20, 1].

A promising direction for further research is the incorporation of spatial effects based on geographical

---

\*Corresponding author: taban.baghfalaki@manchester.ac.uk

regions, an area that has been relatively underexplored [37, 38, 40]. Although joint modeling is highly effective, challenges remain in parameter estimation, which frequently involve complex and time-consuming computations. In the realm of joint modeling, various strategies for parameter estimation are employed. Classical approaches, such as the EM algorithm [31, 21, 27, 39, 41], have been widely utilized alongside Bayesian methods [1]. However, these methods often involve intricate and time-consuming computations, prompting the exploration of alternative strategies. To address this, researchers have explored approximate Bayesian methods as an efficient alternative to traditional approaches [58, 3, 42, 51].

Approximate Bayesian methods are often employed when exact Bayesian inference becomes computationally prohibitive due to the complexity or dimensionality of the model. Several approaches exist to address these challenges. Markov Chain Monte Carlo (MCMC) methods are a widely used class of algorithms that generate samples from the posterior distribution. However, while flexible, they can be computationally intensive, especially in high-dimensional settings [25]. Approximate Bayesian Computation (ABC) is another approach designed for models with intractable likelihoods, where inference is performed by comparing observed data to data simulated under the model [6, 52]. ABC is often applied in fields such as genetics and ecology, where exact likelihood functions are unavailable.

Alternatively, methods such as Variational Inference (VI) and Integrated Nested Laplace Approximation (INLA) offer more computationally efficient solutions. VI approximates the posterior by finding a simpler distribution that minimizes the divergence from the true posterior, often at the cost of some accuracy [9]. INLA, on the other hand, is particularly effective for latent Gaussian models, using Laplace approximations to provide fast and accurate approximations of marginal posteriors [47, 48].

In this paper, we propose an approximate Bayesian method for joint modeling of longitudinal and spatial survival data. Our approach builds upon existing models while introducing innovations to enhance computational efficiency and model flexibility. Performance evaluation through simulation studies and application to real-world HIV/AIDS data from Brazil underscores the utility of our method. For implementation, we leverage the INLA package, which allows for efficient Bayesian inference using Integrated Nested Laplace Approximations. The INLA framework is particularly well-suited for high-dimensional latent models like those involving spatial and longitudinal data. Additionally, we provide accompanying R code to ensure reproducibility and facilitate the application of our method in other research settings. By combining the strengths of INLA with our methodological enhancements, our approach offers a robust and computationally feasible solution to the challenges of joint modeling in complex data scenarios.

We employ an approximate Bayesian approach to implement joint modeling of longitudinal and spatial survival data. While the core model resembles that of [38], we introduce two key innovations: (1) leveraging approximate Bayesian inference instead of the traditional MCMC method, resulting in reduced computational time compared to Gibbs sampling, and (2) incorporating a partial linear joint model to account for nonlinear effects of time, thereby enhancing model versatility. To evaluate the performance of our proposed model, we conduct simulation studies and apply it to real-world Brazilian HIV/AIDS data. We utilize the INLA package for implementation, and the accompanying R code is publicly available at <https://github.com/tbaghfalaki/ASJM>.

The structure of this paper is organized as follows: Section 2 details the specification of the joint modeling framework, including longitudinal submodels, spatial survival submodel, and the approximate Bayesian approach for model implementation. Section 3 focuses on the analysis of real data, while Section 4 presents the results of simulation studies. Finally, Section 5 provides concluding remarks and discusses avenues for future research.

## 2 Joint modeling specification

### 2.1 Notation

The spatial joint model has two separate submodels including a linear mixed effects model and a spatial survival model. The association of these two separate models are taken into account by a shared random effect. Let  $N$  individuals be collected from  $K$  regions such that the number of individuals in each region is  $n_k$  and  $\sum_{k=1}^K n_k = N$ .

Let  $T_{ik}^*$  be the true value of survival time for the  $i^{th}$  individual in the  $k^{th}$  region, such that the observed

survival time  $T_{ik}$  is the minimum value of  $T_{ik}^*$  and the censoring time  $C_{ik}$ , that is,  $T_{ik} = \min(T_{ik}^*, C_{ik})$ . Consider an indicator  $\delta_{ik}$  such that  $\delta_{ik} = 0$  indicates a right censored observation. Thus, the survival outcome is the pair  $(T_{ik}, \delta_{ik})$ ,  $i = 1, \dots, n_k, k = 1, \dots, K$ .

The longitudinal outcomes for each individual are collected at time points  $s_{ikj} < T_{ik}$ ,  $i = 1, \dots, n_k, k = 1, \dots, K, j = 1, \dots, m_{ik}$ , where  $m_{ik}$  is the number of repeated measurements for the  $i^{\text{th}}$  individual in the  $k^{\text{th}}$  region. Therefore, the observed vector of longitudinal outcome is given by  $\mathbf{y}_{ik} = (y_{ik1}, \dots, y_{ikm_{ik}})'$ , where  $y_{ikj} = y_{ik}(s_{ikj})$  and it is obtained as the sum of the true value of the longitudinal outcome at the same time point,  $y_{ik}^*(s_{ikj})$ , and an error term, that is,  $y_{ik}(s_{ikj}) = y_{ik}^*(s_{ikj}) + \epsilon_{ik}(s_{ikj})$ .

## 2.2 Longitudinal submodel

We consider a semi-parametric mixed effects model for describing the longitudinal process as follows

$$y_{ik}(s_{ikj}) = y_{ik}^*(s_{ikj}) + \epsilon_{ik}(s_{ikj}) = \mathbf{x}'_{1ik}(s_{ikj})\boldsymbol{\beta} + g(s_{ikj}) + \mathbf{z}'_{ik}(s_{ikj})\mathbf{b}_{ik} + \epsilon_{ik}(s_{ikj}), \quad (1)$$

where  $\mathbf{x}_{1ik}(s)$  is a  $p_1$ -dimensional vector of explanatory variables at time point  $s$  corresponding to the regression coefficients  $\boldsymbol{\beta}$ ,  $\mathbf{z}_{ik}(s)$  denotes a  $q$ -dimensional vector of explanatory variables at time point  $s$  corresponding to the random effects  $\mathbf{b}_{ik}$ ,  $\mathbf{b}_{ik} \sim N_q(\mathbf{0}, \mathbf{D})$ ,  $\epsilon_{ik}(s)$ s are the error terms which are assumed to be independently and identically distributed as  $N(0, \sigma^2)$  and  $g(s)$  is a nonlinear function. The shape of  $g(\cdot)$  is typically unknown and it should be estimated using some semi-parametric approaches such as spline functions.

The spline function with fixed knots sequence  $\kappa_1 < \dots < \kappa_l$  and fixed degree  $d$  can be given by:

$$g(s) = \sum_{j=1}^{l+d+1} \alpha_j^* B_j(s), \quad (2)$$

where  $B_j$ s are basis functions defining a vector space and  $\alpha_j^*$ s are the associated spline coefficients. Some of the possible basis functions are the truncated power basis, the B-spline basis and the natural spline. For more details see [61] and [3].

The number and the positions of the knots are important issues of the spline function. The use of a penalized spline is a popular strategy for this purpose [61]. Another strategy for this aim is to determine the optimal number of knots by using, for instance, generalized cross validation, AIC, etc. [17, 61]. For considering the spline function INLA in software R mentioning the knots, giving the degree and adding the basis functions as some new covariates to the model are necessary [59].

## 2.3 Spatial survival submodel

For the survival outcome, a proportional hazard model considered as follows:

$$h_{ik}(t) = h_{0i}(t) \exp \{ \mathbf{x}_{2ik}(t)' \boldsymbol{\alpha} + \boldsymbol{\gamma}' \mathbf{b}_{ik} + \nu_k \}, \quad (3)$$

where  $\mathbf{x}_{2ik}(t)$  is the  $p_2$ -dimensional vector of explanatory variables,  $\boldsymbol{\alpha}$  is the fixed effects corresponding to  $\mathbf{x}_{2ik}(t)$ ,  $\boldsymbol{\gamma}$  denotes a vector of the parameters for measuring the association between two models,  $h_{0i}(t) = \varphi t^{\varphi-1}$ ,  $\varphi > 0$  which leads to Weibull hazard function and  $\nu_k$ , for  $k = 1, \dots, K$  represent spatial random effects. Although, we consider only the Weibull hazard function, because of its simplicity, other forms might be considered as well.

A proper non-intrinsic Besag model [7, 8] is applied to consider such that the conditional distribution of each areal unit given the other units is defined as:

$$\nu_k | \boldsymbol{\nu}_{-k} \sim N \left( \frac{1}{n_k} \sum_{k \sim k'} \nu_{k'}, \frac{1}{\tau n_k} \right), \quad (4)$$

where  $n_k$  is the number of neighbors of region  $k$ ,  $\boldsymbol{\nu} = (\nu_1, \dots, \nu_K)'$ ,  $k \sim k'$  indicates that the two regions  $k$  and  $k'$  are neighbors (i.e., they share a boundary or are adjacent to each other),  $\boldsymbol{\nu}_{-k} =$

$(\nu_1, \dots, \nu_{k-1}, \nu_{k+1}, \dots, \nu_K)'$  represents the vector of values from all regions except region  $k$ , and  $\tau > 0$  is a scaling parameter, also referred to as the precision parameter.

This equation describes the conditional distribution of  $\nu_k$  (the value of the spatial variable in region  $k$ ) given all other values  $\boldsymbol{\nu}_{-k}$ . It follows a normal distribution where the mean is the average value of the neighboring regions  $k'$ , weighted by the number of neighbors  $n_k$ . The variance of the conditional distribution is inversely proportional to both the number of neighbors  $n_k$  and the precision parameter  $\tau$ .

This setup implies that the value of  $\nu_k$  depends primarily on the values of its neighboring regions and suggests that areas with more neighbors will have a more tightly constrained (lower variance) value for  $\nu_k$ . This conditional distribution is a key element of the Gaussian Markov Random Field (GMRF) structure, where each region is conditionally dependent on its neighbors.

By considering Brook's lemma [10], given the  $K$  normal full conditional (4),  $\boldsymbol{\nu}$  is a Gaussian Markov random field [50, 49, GMRF] with mean  $\mathbf{0}$  and precision matrix  $\tau\boldsymbol{\Omega}$ , being its entries defined as  $\omega_{kk} = n_k$  and  $\omega_{kj} = 1, k \neq j$ . We can use the following notation instead:

$$\boldsymbol{\nu} \sim N_K(\mathbf{0}, \tau^{-1}\boldsymbol{\Omega}^{-1}). \quad (5)$$

Here,  $\boldsymbol{\nu} = (\nu_1, \dots, \nu_K)'$  is the vector representing the spatial variable in each of the  $K$  regions. The notation  $\boldsymbol{\nu} \sim N_K(\mathbf{0}, \tau^{-1}\boldsymbol{\Omega}^{-1})$  indicates that  $\boldsymbol{\nu}$  follows a multivariate normal distribution with mean  $\mathbf{0}$  and a precision matrix  $\tau\boldsymbol{\Omega}$ .

- $\tau^{-1}$  is the scaling parameter (the inverse of the precision parameter  $\tau$ ).
- $\boldsymbol{\Omega}$  is the precision matrix, which encodes the spatial dependencies between regions. The structure of  $\boldsymbol{\Omega}$  is based on the neighborhood system of the regions:
- $\omega_{kk} = n_k$ , the number of neighbors for region  $k$ ,
- $\omega_{kj} = 1$  if regions  $k$  and  $j$  are neighbors,
- $\omega_{kj} = 0$  if regions  $k$  and  $j$  are not neighbors.

This precision matrix  $\boldsymbol{\Omega}$  ensures that the spatial dependencies are captured properly, as it reflects the strength of the relationships between neighboring regions. A high precision value means stronger dependency, while regions that are not neighbors will have no direct dependency (i.e.,  $\omega_{kj} = 0$ ).

In this paper, we use the second proper version of the Besag model [50] as the distributional assumption for  $\boldsymbol{\nu}$  which is corrected by a ratio  $\zeta \in (0, 1)$  as follows:

$$\boldsymbol{\nu} \sim N_K(\mathbf{0}, \tau^{-1}((1 - \zeta)\mathbf{I}_K + \zeta\boldsymbol{\Omega}^{-1})), \quad (6)$$

where  $\mathbf{I}_K$  is a  $K \times K$  identity matrix.

This equation introduces a correction to the standard Besag model. The parameter  $\zeta$  is used to adjust the influence of the spatial structure (encoded in  $\boldsymbol{\Omega}$ ) versus independent variability (encoded in  $\mathbf{I}_K$ , the identity matrix).

- $\mathbf{I}_K$  is the identity matrix of size  $K \times K$ , which represents independent variation for each region. If only  $\mathbf{I}_K$  were present (i.e.,  $\zeta = 0$ ), it would imply no spatial dependence, and each region would have an independent normal distribution with variance  $\tau^{-1}$ .
- $\boldsymbol{\Omega}^{-1}$  represents the spatial structure, where  $\boldsymbol{\Omega}$  is the precision matrix derived from the neighborhood relationships of the regions.
- The term  $(1 - \zeta)\mathbf{I}_K + \zeta\boldsymbol{\Omega}^{-1}$  is a weighted combination of the identity matrix and the inverse precision matrix, allowing a balance between independent variation and spatial dependence. The parameter  $\zeta$  controls this balance:
- When  $\zeta = 1$ , the model fully depends on the spatial structure (as in the original Besag model).
- When  $\zeta = 0$ , the model implies no spatial correlation, and the regions are modeled independently.

This modification is essential to ensure the model is proper (i.e., the covariance matrix is positive definite) and that the spatial structure is still retained, but in a controlled manner. The model remains flexible, as  $\zeta$  can be tuned to allow for different levels of spatial dependence in the data.

## 2.4 Approximate Bayesian approach

In this section, we use the approximate Bayesian approach to perform inference for the spatial joint model. For this aim, at the first stage we specify the spatial joint model in term of latent Gaussian

models (LGM), then we apply integrated nested Laplace approximation (INLA) to approximate the joint posterior density of the model.

### Spatial joint model in term of latent Gaussian models

Let  $\eta_{ikj}^y$  denote the latent variable for the longitudinal outcome of the  $i^{th}$  individual in the  $k^{th}$  region at time  $s_{ikj}$ , defined as

$$\eta_{ikj}^y = \mathbf{x}'_{1ik}(s_{ikj})\boldsymbol{\beta} + g(s_{ikj}) + \mathbf{z}'_{ik}(s_{ikj})\mathbf{b}_{ik}.$$

The latent variable for the survival outcome of the same individual is

$$\eta_{ik}^t = \mathbf{x}_{2ik}(t)'\boldsymbol{\alpha} + \boldsymbol{\gamma}'\mathbf{b}_i + \nu_k.$$

The vectors  $\boldsymbol{\eta}_{ik}^y = (\eta_{i11}^y, \dots, \eta_{ikm_{ik}}^y)$  and  $\boldsymbol{\eta}_k^y = (\eta_{1k}^y, \dots, \eta_{n_k, k}^y)$  summarize the longitudinal latent variables for individuals and regions, while  $\boldsymbol{\eta}_k^t = (\eta_{1k}^t, \dots, \eta_{n_k, k}^t)$  captures the survival latent variables for the  $k^{th}$  region. The overall observed longitudinal outcomes are represented by  $\mathbf{y} = (\mathbf{y}_{11}, \dots, \mathbf{y}_{n_K K})$ , the observed survival times by  $\mathbf{T} = (T_{11}, \dots, T_{n_K K})$ , and the censoring indicators by  $\boldsymbol{\delta} = (\delta_{11}, \dots, \delta_{n_K K})$ . The covariate matrices are defined as  $\mathbf{x}_1 = (\mathbf{x}_{111}, \dots, \mathbf{x}_{1n_K K})$  for longitudinal outcomes and  $\mathbf{x}_2 = (\mathbf{x}_{211}, \dots, \mathbf{x}_{2n_K K})$  for survival analysis, while  $\mathbf{z} = (\mathbf{z}_{11}, \dots, \mathbf{z}_{n_K K})$  contains random effects covariates. Additionally, let  $\boldsymbol{\theta}_1$  be the vector of hyperparameters, and  $\boldsymbol{\Lambda} = \{\boldsymbol{\eta}_1, \dots, \boldsymbol{\eta}_K, \boldsymbol{\beta}, \boldsymbol{\alpha}, \boldsymbol{\gamma}\}$  represent the latent structure, which is considered a GMRF.  $\boldsymbol{\eta}$  is specified as a latent Gaussian random field with the following density function:

$$\boldsymbol{\eta}|\boldsymbol{\theta}_1 \sim N(\mathbf{0}, Q^{-1}(\boldsymbol{\theta}_1)) \quad (7)$$

where  $Q(\boldsymbol{\theta}_1)$  is a sparse precision matrix with a vector of parameters  $\boldsymbol{\theta}_2$ .

The joint distribution (likelihood function) of  $\mathbf{y}, \mathbf{T}$  and  $\boldsymbol{\delta}$  given  $\boldsymbol{\Lambda}, \boldsymbol{\theta}_2, \mathbf{x}_1, \mathbf{x}_2$  and  $\mathbf{z}$  is as follows

$$\begin{aligned} \pi(\mathbf{y}, \mathbf{T}, \boldsymbol{\delta}|\boldsymbol{\Lambda}, \boldsymbol{\theta}_2, \mathbf{x}_1, \mathbf{x}_2, \mathbf{z}) &= \prod_{k=1}^K \prod_{i=1}^{n_k} \prod_{j=1}^{m_{ik}} \phi(y_{ikj}; \eta_{ikj}^y, \sigma^2) \\ &\times \prod_{k=1}^K \prod_{i=1}^{n_k} h_{ik}(t)^{\delta_{ik}} \exp\left\{-\int_0^{T_{ik}} h_{ik}(s)ds\right\}. \end{aligned} \quad (8)$$

where  $\phi(\cdot; \mu, \sigma^2)$  denotes the normal distribution with mean  $\mu$  and variance  $\sigma^2$ ,  $h_{ik}(t) = h_{0i}(t) \exp(\eta_{ik}^t)$  is the hazard function given by (3) and  $\boldsymbol{\theta}_1 = \{\sigma^2, \boldsymbol{\varphi}\}$ .

Note that this likelihood is obtained by the assumption of the joint modeling: given the random effects  $\mathbf{b}_{ik}$ , the random variables  $\mathbf{y}_{ik}$  and  $(T_{ik}, \delta_{ik})$  are independent. Also, given  $\mathbf{b}_{ik}$ , the components of  $y_{ik1}, \dots, y_{ikm_{ik}}$  are independent.

Consider a prior  $\pi(\boldsymbol{\theta})$  for  $\boldsymbol{\theta} = (\boldsymbol{\theta}_1, \boldsymbol{\theta}_2)$ . The joint posterior distribution of  $\boldsymbol{\Lambda}$  and  $\boldsymbol{\theta}$  given  $\mathbf{y}, \mathbf{t}$  and  $\boldsymbol{\delta}$  is as follows:

$$\pi(\boldsymbol{\Lambda}, \boldsymbol{\theta}|\mathbf{y}, \mathbf{t}, \boldsymbol{\delta}) \propto \pi(\mathbf{y}, \mathbf{T}, \boldsymbol{\delta}|\boldsymbol{\Lambda}, \boldsymbol{\theta}_1, \mathbf{x}_1, \mathbf{x}_2, \mathbf{z})\pi(\boldsymbol{\Lambda}|\boldsymbol{\theta}_2)\pi(\boldsymbol{\theta}). \quad (9)$$

The strategy of INLA is to estimate the marginal distributions of the latent effects and the hyperparameters. For a latent parameter  $\Lambda_j$ , we have

$$\pi(\Lambda_j|\mathbf{y}, \mathbf{t}, \boldsymbol{\delta}) = \int \pi(\Lambda_j|\boldsymbol{\theta}, \mathbf{y}, \mathbf{t}, \boldsymbol{\delta})\pi(\boldsymbol{\theta}|\mathbf{y}, \mathbf{t}, \boldsymbol{\delta})d\boldsymbol{\theta}. \quad (10)$$

Also, the posterior marginal for a hyperparameter  $\theta_k$  is as follows:

$$\pi(\theta_j|\mathbf{y}, \mathbf{t}, \boldsymbol{\delta}) = \int \pi(\boldsymbol{\theta}|\mathbf{y}, \mathbf{t}, \boldsymbol{\delta})d\boldsymbol{\theta}_{-j}. \quad (11)$$

where  $\boldsymbol{\theta}_{-j}$  is a vector of hyperparameters  $\boldsymbol{\theta}$  without  $\theta_j$ .

Based on the approximation of [50], the joint posterior distribution of  $\boldsymbol{\theta}$ ,  $\tilde{\pi}(\boldsymbol{\theta}|\mathbf{y}, \mathbf{t}, \boldsymbol{\delta})$ , can be used to compute equations (10) and (11) as follows:

$$\tilde{\pi}(\boldsymbol{\theta}|\mathbf{y}, \mathbf{t}, \boldsymbol{\delta}) \propto \frac{\pi(\boldsymbol{\Lambda}, \boldsymbol{\theta}, \mathbf{y}, \mathbf{t}, \boldsymbol{\delta})}{\tilde{\pi}_G(\boldsymbol{\Lambda}|\boldsymbol{\theta}, \mathbf{y}, \mathbf{t}, \boldsymbol{\delta})} \Bigg|_{\boldsymbol{\Lambda}=\boldsymbol{\Lambda}^*(\boldsymbol{\theta})}, \quad (12)$$

where  $\tilde{\pi}_G(\Lambda|\boldsymbol{\theta}, \mathbf{y}, \mathbf{t}, \boldsymbol{\delta})$  is a Gaussian approximation of  $\pi_G(\Lambda|\boldsymbol{\theta}, \mathbf{y}, \mathbf{t}, \boldsymbol{\delta})$  and  $\Lambda^*(\boldsymbol{\theta})$  is the mode of this distribution for a given value of  $\boldsymbol{\theta}$ . The posterior marginal distribution of  $\pi(\theta_j|\mathbf{y}, \mathbf{t}, \boldsymbol{\delta})$  can be approximated by integrating  $\boldsymbol{\theta}_{-j}$  out in equation (12).

**Approximations for  $\pi(\Lambda_j|\boldsymbol{\theta}, \mathbf{y}, \mathbf{t}, \boldsymbol{\delta})$**

The approximation of  $\Lambda_j$  given  $\mathbf{y}, \mathbf{t}, \boldsymbol{\delta}$  in INLA can be obtained by the following expression:

$$\pi(\Lambda_j|\mathbf{y}, \mathbf{t}, \boldsymbol{\delta}) \simeq \sum_{r=1}^R \tilde{\pi}(\Lambda_j|\boldsymbol{\theta}^{(r)}, \mathbf{y}, \mathbf{t}, \boldsymbol{\delta}) \tilde{\pi}(\boldsymbol{\theta}^{(r)}|\mathbf{y}, \mathbf{t}, \boldsymbol{\delta}) \Delta_r, \quad (13)$$

where  $\{\boldsymbol{\theta}^{(1)}, \dots, \boldsymbol{\theta}^{(R)}\}$  is a set of value of  $\boldsymbol{\theta}$  for computing the numerical integration with weights  $\{\Delta_1, \dots, \Delta_R\}$ .

The three different following approximations are described by [50] to approximate  $\pi(\Lambda_j|\boldsymbol{\theta}, \mathbf{y}, \mathbf{t}, \boldsymbol{\delta})$ :

1. Marginalization of the denominator of equation (12).
2. The use of the Laplace approximation as follows:

$$\pi_{LA}(\Lambda_j|\boldsymbol{\theta}, \mathbf{y}, \mathbf{t}, \boldsymbol{\delta}) \propto \frac{\pi(\Lambda, \boldsymbol{\theta}, \mathbf{y}, \mathbf{t}, \boldsymbol{\delta})}{\pi_G(\Lambda_{-j}|\Lambda_j, \boldsymbol{\theta}, \mathbf{y}, \mathbf{t}, \boldsymbol{\delta})} \Big|_{\Lambda_{-j}=\Lambda_{-j}^*(\Lambda_j, \boldsymbol{\theta})},$$

where  $\pi_G(\Lambda_{-j}|\Lambda_j, \boldsymbol{\theta}, \mathbf{y}, \mathbf{t}, \boldsymbol{\delta})$  is the Gaussian approximation for  $\pi(\Lambda_{-j}|\Lambda_j, \boldsymbol{\theta}, \mathbf{y}, \mathbf{t}, \boldsymbol{\delta})$  and  $\Lambda_{-j} = \Lambda_{-j}^*(\Lambda_j, \boldsymbol{\theta})$  is its mode. This methodology is computationally expensive, thus, the following approximation is proposed:

$$\pi_{LA}(\Lambda_j|\boldsymbol{\theta}, \mathbf{y}, \mathbf{t}, \boldsymbol{\delta}) \propto \phi(\Lambda_j; \mu_j^\Lambda(\boldsymbol{\theta}), \sigma_j^\Lambda(\boldsymbol{\theta})) \times \exp(CS(\Lambda_j)),$$

where  $CS(\Lambda_j)$  denotes a cubic spline on  $\Lambda_j$  with the aim to correct the approximation.

3. The third approach is the simplified Laplace approximation and it is based on a series of expansions of  $\pi_{LA}(\Lambda_j|\boldsymbol{\theta}, \mathbf{y}, \mathbf{t}, \boldsymbol{\delta})$  around  $\Lambda_j = \mu_j^\Lambda(\boldsymbol{\theta})$ . This approach is very fast and the use of it can correct the location and scale of Gaussian approximation.

### 3 Analysis of the HIV/AIDS data

#### 3.1 Data description

Three major electronic databases are maintained by the Brazilian National AIDS Program [19]: (i) SINAN-AIDS (Information System for Notifiable Diseases of AIDS Cases), the most important electronic AIDS surveillance database, which contains all reported cases since 1980; (ii) SISCEL (Laboratory Test Control System), designed to monitor laboratory tests such as CD4 counts and viral load tests for HIV/AIDS patients in the public health sector since 2002; and (iii) SICLOM (System for Logistic Control of Drugs) was developed to manage the logistics of AIDS treatment deliveries. Since 2002, it has been sharing the patient list with SISCEL. These three databases have previously been merged into a single database containing both HIV and AIDS cases using a process called record linkage, which was implemented by the Surveillance Unit of the Brazilian National AIDS Program [19]. This linkage strategy has been increasingly used in AIDS surveillance and research [16] to verify underreporting of cases and eliminate duplicates. In Brazil, this procedure has improved the quality of HIV/AIDS data information [19]. Notice that the period from 2002 to 2006 can be considered the first period with substantial information on both HIV/AIDS survival and CD4 exams. During this period, 88 laboratories across all 27 Brazilian states were utilizing SISCEL, encompassing 90% of all CD4 and viral load tests conducted by the public health sector. Cases diagnosed before 2002 were excluded because personal identifiers were not available in the mortality database for the entire country before that date [19]. For institutional reasons, we only had access to a simple random sample of the combined database, which will be referred to as the HIV/AIDS data [37, 38]. The dataset consists of 500 random samples, denoted as N=500, from the original data. The explanatory variables in this study include age (1: older than 50, 0: younger than 50), gender (1: male, 0: female), PrevOI (1: with PrevOI, 0: without PrevOI), and time.

Figure 1 presents the Kaplan-Meier survival curve illustrating mortality over a five-year follow-up in HIV/AIDS data. The data includes 34 deaths, accounting for 93.2% of the right-censored cases. There are 298 (59.6%) male patients, 60 (12%) of whom are older than 50, and 198 (39.6%) have a history of previous infection. The study includes 2757 longitudinal observations, with an average of 5.51 replications for each patient. The average time for censored patients is 997.9 days, whereas for the others, it is 862.4 days. On average, there are 18.52 patients with a standard deviation of 41.08 in each of the 27 Brazilian states. Additionally, two states have no patients in this dataset.

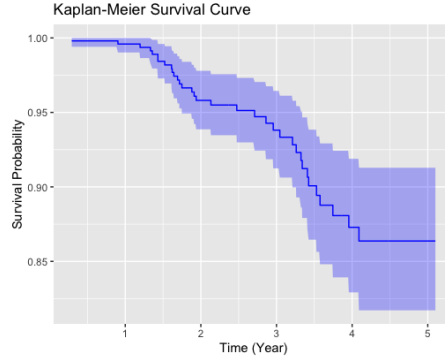


Figure 1: Kaplan-Meier survival curve for mortality over five years of follow-up in HIV/AIDS data.

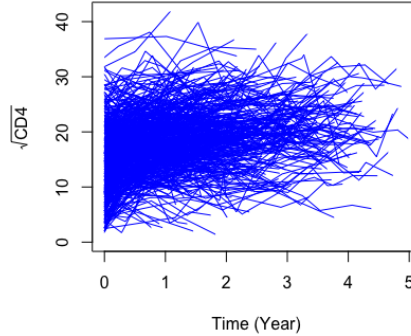


Figure 2: Individual trajectories of the square root of CD4 levels over time in HIV/AIDS longitudinal data.

### 3.2 Data analysis

In this section, the proposed methodology described in Section 3 is used to analysis the HIV/AIDS data. As in [37] and [38], the response variable is defined to be  $\sqrt{CD4}$  in order to deal with the asymmetry in the longitudinal measurements. Figure 2 presents individual trajectories of square root-transformed CD4 counts over time in the HIV/AIDS dataset. Let  $Y_{ikj}$  denote the response variable for the  $j^{th}$  time point of the  $i^{th}$  patient in the  $k^{th}$  state,  $k = 1, \dots, K$ . The following longitudinal model is considered to analyse the data:

$$Y_{ikj} = \beta_0 + \beta_1 \text{Age}_{ik} + \beta_2 \text{Gender}_{ik} + \beta_3 \text{PrevOI}_{ik} + g(s_{ikj}) + \mathbf{z}'_{ik}(s_{ikj})\mathbf{b}_{ik} + \epsilon_{ikj}, \quad (14)$$

Also, for survival time, the following model is considered:

$$h(t_{ik}) = h_0(t_{ik}) \exp(\alpha_0 + \alpha_1 \text{Age}_{ik} + \alpha_2 \text{Gender}_{ik} + \alpha_3 \text{PrevOI}_{ik} + \boldsymbol{\gamma}' \mathbf{b}_{ik} + \nu_k) \quad (15)$$

where  $\epsilon_{ikj} \sim N(0, \sigma^2)$ ,  $(b_{ik0}, b_{ik1})' \sim N_2(\mathbf{0}, \mathbf{D})$ ,  $g(s_{ikj})$  is a non-linear function of time,  $h_0(t_{ik}) = r t_{ik}^{r-1}$  and  $\nu_k$  is distributed as in (4). A variety of fitted joint models with different forms for the longitudinal association  $(\mathbf{z}'_{ik}(s_{ikj}) \mathbf{b}_{ik})$ , for the linkage structure  $(\boldsymbol{\gamma}' \mathbf{b}_{ik})$  and for the spatial random effects  $(\nu_k)$  are considered. Table 1 reports the values of DIC and WAIC for purposes of the model comparison. Based on the results, model xi with  $\mathbf{z}'_{ik}(s_{ikj}) = b_{ik0} + b_{ik1} s_{ikj}$ ,  $\boldsymbol{\gamma}' \mathbf{b}_{ik} = \gamma_1 b_{ik0} + \gamma_2 b_{ik1}$  and by considering  $\nu_k$  as the spatial random effects is the best fitting model. The results of this model can be found in Table 2. Dimensionality of the basis (i.e.: number of knots + degree) for the B-spline is considered to be equal to 5. The results in this table show that age, time and PrevOI are significant variables in the longitudinal model such that the older people or having PrevOI lead to smaller values of CD4 count measurements. Also, PrevOI is a significant variable in the survival model.  $\gamma_1$  and  $\gamma_2$  are also significant which confirms the association between two outcomes.

In Figure 3, patient-specific predictions [58] for longitudinal trajectories and survival functions are depicted for three randomly selected patients. The left panel displays the observed values of  $\sqrt{CD4}$  for each patient, represented by solid black lines, alongside their corresponding model-based predictions shown as blue dashed lines. The close proximity of these lines suggests high accuracy in the predictions. In the right panel of Figure 3, the survival curves superimposed by median lines for each patient are also given. For model assessment and checking adequacy of the models, in addition of comparison between predicted values and observed values, a residual analysis is performed. For the residual analysis of the longitudinal component, the standardized marginal residuals are computed as

$$e_{ikj}^{sm} = \frac{Y_{ikj} - \hat{\eta}_{ikj}^y}{\sqrt{\mathbf{z}'_{ik}(s_{ikj}) \hat{\mathbf{D}} \mathbf{z}_{ik}(s_{ikj}) + \hat{\sigma}^2}},$$

where,  $\hat{\eta}_{ikj}^y = \hat{\beta}_0 + \hat{\beta}_1 \text{Age}_{ik} + \hat{\beta}_2 \text{Gender}_{ik} + \hat{\beta}_3 \text{PrevOI}_{ik} + \hat{g}(s_{ikj})$ , such that  $\hat{\beta}_k$ ,  $k = 0, \dots, 3$  are estimated values of their parameters,  $\hat{\mathbf{D}}$  and  $\hat{\sigma}^2$  are estimated values of  $\mathbf{D}$  and  $\sigma^2$ , respectively and  $\hat{g}(s_{ikj})$  is the estimated spline function. Panel (b) of Figure 4 shows the standardized marginal residuals and supports the goodness of fit of the model.

For the residuals analysis of the spatial survival model, the Cox-Snell residuals are considered [15]. We have  $r_{ik}^{CS}(t|\boldsymbol{\theta}) = -\log S(t_{ik}|\boldsymbol{\theta})$  which can be calculated by the expected value over the posterior distribution as follows [45]:

$$r_{ik}^{CS}(t) = \int r_{ik}^{CS}(t|\boldsymbol{\theta}) \pi(\boldsymbol{\theta}|\mathbf{t}, \mathbf{y}) d\boldsymbol{\theta},$$

In practice,  $r_{ik}^{CS}(t)$  can be computed at the observed survival time  $t_{ik}$ . For checking the fit of the survival model, taking into account the censoring time, the associated Kaplan–Meier estimate of the  $r_{ik}^{CS}(t)$  is compared with the survival function of the unit exponential distribution [15]. The plot of the Cox-Snell residuals is presented in Figure 5. The closeness of the two curves confirms the goodness of fit of the proposed survival model in the joint model.

Figure 6 shows two maps for the HIV/AIDS data of Brazilian states using model xi. The left panel of this figure represents the posterior spatial mean risk, that is, if we define  $\hat{\lambda}_{ik} = \hat{\alpha}_0 + \hat{\alpha}_1 \text{Age}_{ik} + \hat{\alpha}_2 \text{Gender}_{ik} + \hat{\alpha}_3 \text{PrevOI}_{ik} + \hat{\boldsymbol{\gamma}}' \hat{\mathbf{b}}_{ik} + \hat{\nu}_k$ , then the posterior spatial mean risk for each region is  $\hat{\lambda}_k = \frac{\sum_{i=1}^{n_k} \hat{\lambda}_{ik}}{n_k}$ ,  $k = 1, \dots, K = 27$ . In this equation the hat sign for parameters denotes the approximate Bayesian estimate and the hat sign for random effects denotes the predicted values. The right panel of this figure shows the mean of the predicted values for  $\exp(\nu_k)$ ,  $k = 1, \dots, K = 27$ . The map of the relative risks shows that the states of the north of Brazil have higher level of HIV/AIDS risks. This conclusion was also obtained by [37].

Using a 12th Gen Intel Core i7-12700H processor and 32 GB of RAM, we assessed the computational efficiency of two methods—approximate Bayesian inference via INLA and Gibbs sampling via BUGS—specifically applied to Model xi. The INLA-based approximate Bayes approach completed the



analysis in just 6.287 seconds, illustrating the advantages of a streamlined, highly efficient method well-suited to modern, high-performance hardware. By comparison, Gibbs sampling with 50,000 iterations and two chains in R2OpenBUGS required a considerably longer processing time of 412 minutes (roughly 6.87 hours) to achieve similar results. This striking contrast highlights the computational intensity of Gibbs sampling, particularly in probabilistic frameworks like R2OpenBUGS, where iterative sampling demands extensive processing time. Given these results, we omit further Gibbs sampling outputs to emphasize the efficiency gains achieved with the approximate Bayes approach. The BUGS code for this application can be found in <https://github.com/tbaghfalaki/ASJM>.

Table 1: Model comparison criteria for the candidate joint models.

Model	$z'_{ik}(s_{ikj})\mathbf{b}_{ik}$	$\gamma'\mathbf{b}_{ik}$	$\nu_k$	WAIC	DIC
N	0	0	0	17642	17641
i	$b_{ik0}$	0	0	15193	15171
ii	$b_{ik0}$	$\gamma_1 b_{ik0}$	0	17648	17643
iii	$b_{ik0}$	$\gamma_1 b_{ik0}$	$\nu_k$	15163	15139
iv	0	0	$\nu_k$	17641	17640
v	$b_{ik0} + b_{ik1}s_{ikj}$	$\gamma_1 b_{ik0}$	$\nu_k$	14069	14008
vi	$b_{ik0} + b_{ik1}s_{ikj}$	$\gamma_2 b_{ik1}$	$\nu_k$	14047	13989
vii	$b_{ik0} + b_{ik1}s_{ikj}$	$\gamma_1 b_{ik0}$	0	14077	14014
viii	$b_{ik0} + b_{ik1}s_{ikj}$	$\gamma_2 b_{ik1}$	0	14036	13977
ix	$b_{ik0} + b_{ik1}s_{ikj}$	$\gamma_1 b_{ik0} + \gamma_2 b_{ik1}$	0	14033	13976
x	$b_{ik0} + b_{ik1}s_{ikj}$	0	$\nu_k$	14085	14015
xi	$b_{ik0} + b_{ik1}s_{ikj}$	$\gamma_1 b_{ik0} + \gamma_2 b_{ik1}$	$\nu_k$	14025	13967

Table 2: Bayesian parameter estimates, posterior means (standard deviations), and 95% credible intervals for the HIV/AIDS data using model xi.

Parameter	Mean	SD	Credible Interval		Median
			2.5%	97.5%	
$\beta_0$	9.443	0.899	7.68	11.205	9.443
Age ( $\beta_1$ )	-1.442	0.675	-2.766	-0.118	-1.442
Gender ( $\beta_2$ )	-0.821	0.45	-1.704	0.062	-0.821
PrevOI ( $\beta_3$ )	-1.568	0.456	-2.462	-0.675	-1.568
$g(s)$	-34.46	3.989	-42.283	-26.636	-34.459
	11.123	2.414	6.388	15.857	11.123
	-46.778	4.909	-56.403	-37.149	-46.779
$\sigma^{-2}$	0.159	0.006	0.148	0.17	0.159
$\alpha_0$	-5.138	0.407	-5.992	-4.394	-5.118
Age ( $\alpha_1$ )	0.835	0.428	-0.046	1.636	0.849
Gender ( $\alpha_2$ )	0.352	0.377	-0.364	1.117	0.343
PrevOI ( $\alpha_3$ )	0.89	0.366	0.185	1.622	0.885
$r$	1.159	0.027	1.108	1.214	1.159
$\tau^{-1}$	193.241	35.064	127.947	264.402	192.497
$\gamma_1$	-0.138	0.04	-0.218	-0.061	-0.137
$\gamma_2$	-0.376	0.091	-0.555	-0.196	-0.377
$D_{11}^{-1}$	0.039	0.003	0.033	0.045	0.039
$D_{22}^{-1}$	0.168	0.018	0.136	0.207	0.167
$\rho$	-0.354	0.056	-0.457	-0.238	-0.356

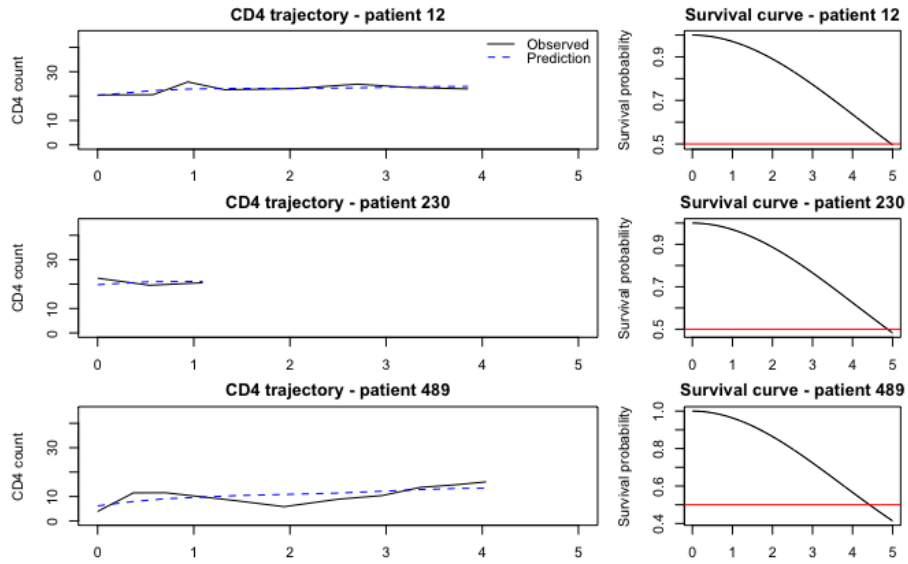


Figure 3: Plots of observed and predicted values for longitudinal outcomes (panel a) and standardized marginal residuals (panel b).

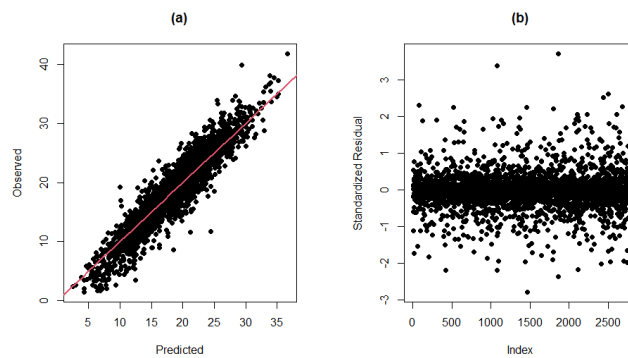


Figure 4: Plots of observed and predicted values for longitudinal outcomes (panel a) and standardized marginal residuals (panel b).

**Survival Function of Cox-Snell Residual**

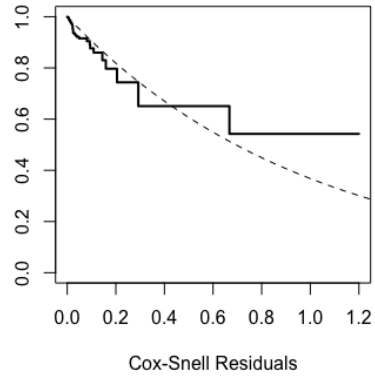


Figure 5: The empirical survival curves based on the Kaplan-Meier posterior estimates of Cox-Snell residuals (solid line) and the unit exponential distribution (dashed line).

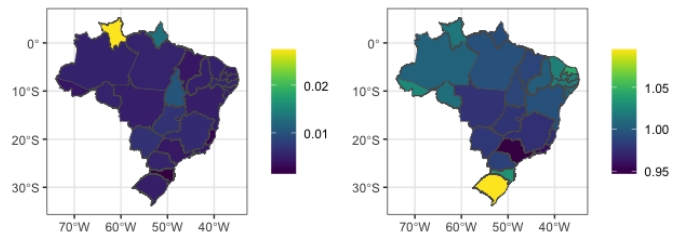


Figure 6: Map of the spatial mean (left panel) and relative risks (right panel) using model xi.

## 4 Simulation studies

### 4.1 Scenario 1

In this section, we conducted simulation studies to assess the performance of the proposed joint model. When considering an areal data set, the shapefile of North Carolina from the `spData`, `maptools`, and `spdep` packages in R is utilized. There are  $K = 100$  regions in this map (see figure 7).

We consider two different levels of sample sizes including  $n_k = 20$  and  $50$ ,  $k = 1, \dots, K$ . We consider two explanatory variables for generating the data:  $\mathbf{x}_1$  is generated from the standard normal distribution as continuous random variable and  $\mathbf{x}_2$  is generated from the Bernoulli distribution with a success probability of 0.5.

The following linear mixed effects model is considered for the longitudinal model:

$$Y_{ikj} = \beta_0 + \beta_1 x_{1ik} + \beta_2 x_{2ik} + g(t_{ikj}) + b_{0ik} + b_{1ik} t_{ikj} + \varepsilon_{ikj}, \quad (16)$$

where  $t_{ik} = (0, 0.05, 0.1, \dots, 1)$ ,  $\boldsymbol{\beta} = (\beta_0, \beta_1, \beta_2)' = (2, -1, 1)'$ ,  $g(t) = \sin(2\pi t)$ ,  $\varepsilon_{ikj} \sim N(0, \sigma^2)$ ,  $\sigma^2 = 1$ ,

$\mathbf{b}_{ik} = (b_{0ik}, b_{1ik})' \sim N_2(\mathbf{0}, \mathbf{D}^{-1})$ , where  $\mathbf{D}^{-1} = \begin{pmatrix} D_{11}^{-1} & \frac{\rho}{\sqrt{D_{11}^{-1} D_{22}^{-1}}} \\ \frac{\rho}{\sqrt{D_{11}^{-1} D_{22}^{-1}}} & D_{22}^{-1} \end{pmatrix}$  is the precision matrix such

that  $\mathbf{D} = \begin{pmatrix} 1 & 0.5 \\ 0.5 & 1 \end{pmatrix}$ . For the survival time the following model is considered:

$$h_{ik}(t) = h_{0ik}(t) \exp(\alpha_0 + \alpha_1 x_{1ik} + \gamma_1 b_{0ik} + \gamma_2 b_{1ik} + \nu_k), \quad (17)$$

where  $\boldsymbol{\alpha} = (\alpha_0, \alpha_1)' = (0.5, -0.5)'$ ,  $\gamma_1 = 1$ ,  $\gamma_2 = -1$ ,  $h_{0ik}(t) = \varpi t^{\varpi-1}$ ,  $\varpi = 1$  and 40% rate of right censoring is considered. For generating  $\boldsymbol{\nu} = (\nu_1, \dots, \nu_K)'$ , equation (4) is considered such that  $\tau = 0.1$ . The following four models are assessed with  $M = 200$  replications:

**Model I** Separate models without spatial random effects.

**Model II** Separate models with spatial random effects.

**Model III** Joint model without spatial random effects.

**Model IV** Joint model with spatial random effects.

The first two models ignore the joint analysis of two outcomes. The first and the third ones ignore the spatial effects and model IV is the model by considering spatial effects and joint analysis. For model comparison relative bias and root of mean squared errors are used such that  $Rbias(\vartheta) = \frac{\bar{\hat{\vartheta}}}{\vartheta} - 1$ ,

$RMSE(\vartheta) = \sqrt{\frac{\sum_{l=1}^M (\hat{\vartheta}_l - \vartheta)^2}{M}}$ , where  $\hat{\vartheta}_l$  is the estimated value of parameter  $\vartheta$  for the  $l$ th simulation run and

$\bar{\hat{\vartheta}} = \frac{\sum_{l=1}^M \hat{\vartheta}_l}{M}$ . Also, DIC and WAIC are utilized for selecting the best-fitting model. A difference in DIC greater than 10 is regarded as a strong indicator of model preference, whereas a difference between 5 and 10 suggests meaningful distinctions, indicating that the models may still be comparable [54]. Similarly, for WAIC, a difference of 10 is considered substantial evidence in favor of the model with the lower WAIC [23].

The results shown in Table 3 and Figure 9 indicate that the four models exhibit significant differences in their performance for parameter estimation. Model I (separate models without spatial effects) exhibits the highest bias and RMSE, resulting in unreliable estimates. Model II (separate models with spatial effects) shows some improvement, but its accuracy remains insufficient. In contrast, Model III (joint model without spatial effects) outperforms the separate models; however, neglecting spatial effects can still lead to inaccurate estimates. Model IV (joint model with spatial effects) delivers the best performance by effectively incorporating spatial correlations and jointly analyzing both outcomes. The DIC and WAIC results further reinforce the superiority of Model IV, with substantial differences exceeding 10 in these

metrics, indicating its excellent fit to the data. Overall, Model IV emerges as the optimal choice for the analyzed data, highlighting the critical importance of considering spatial effects and joint analysis for achieving more accurate parameter estimates.

In terms of variance components, the estimates for  $\sigma^2$ ,  $D_{11}^{-1}$ ,  $D_{22}^{-1}$ , and  $\rho$  across all models are close to the true values, with small Rbias and RMSE values reflecting good accuracy. The estimated values of spatial precision ( $\tau^{-1}$ ) for Models II and IV are also close to the true values, with Model IV yielding the closest estimate. The parameters  $\gamma_1$  and  $\gamma_2$  in Model IV are near the true values, whereas Model III shows considerable deviation with larger Rbias and RMSE values. Based on the DIC and WAIC metrics, Model IV is confirmed as the best-fitting model.

A comparison of parameter estimates across different sample sizes indicates that the model with  $n_k = 50$  generally outperforms the one with  $n_k = 20$ . For instance, the relative bias and RMSE for the parameter  $\beta_0$  are lower with  $n_k = 50$  (Rbias = 0.020, RMSE = 0.042) compared to  $n_k = 20$  (Rbias = 0.021, RMSE = 0.047), suggesting improved accuracy in estimation. Although the relative bias for  $\beta_1$  is slightly higher at  $n_k = 50$  (Rbias = 0.005), its RMSE is lower (0.015) compared to  $n_k = 20$  (0.021), indicating better overall precision. The parameter  $\alpha_0$  demonstrates a less negative relative bias with  $n_k = 50$  (-1.199) and a comparable RMSE (0.600), reflecting greater stability. Notably, the RMSE for the variance parameter  $\sigma^2$  shows a significant reduction from  $n_k = 20$  (0.009) to  $n_k = 50$  (0.006), indicating enhanced estimation accuracy. Furthermore, the relative bias for  $D_{11}^{-1}$  is virtually eliminated at  $n_k = 50$  (Rbias = 0.000), with a marked improvement in RMSE from 0.041 to 0.024. Collectively, these findings underscore the importance of larger sample sizes in obtaining more reliable parameter estimates.

This simulation study was conducted on a MacBook Pro 2020, equipped with Apple’s state-of-the-art M1 chip and 256GB of storage. In Table 3, we provide the mean and standard deviation of the computational times measured in minutes. Notably, despite the complexity of the models, the computational times remain relatively short. For more intricate models, although the computational time increases, it typically does not exceed one minute on average for  $n_k = 50$ .

Figure 8 shows plots of the estimated curves superimposed by its 95%CI for the non-linear function of time for  $n_k = 20$  (panel a) and for  $n_k = 50$  (panel b). These figures confirm our discussions about the strategy about the use of a spline function for take into account the non-linear effect of time, i.e., the estimated curves for the B-spline are near to the real curves and by increasing the  $n_k$  the length of their 95%CI decreases.

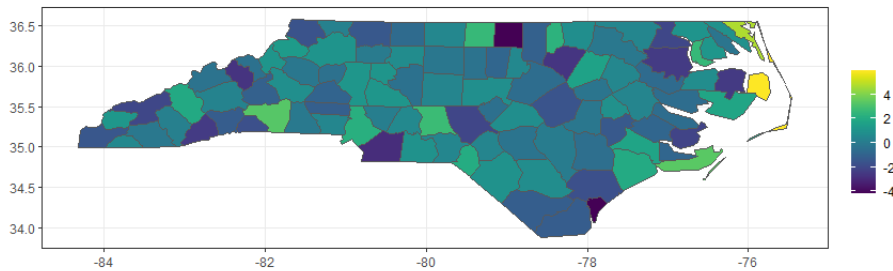


Figure 7: Generated spatial frailties of North Carolina for one replication in the simulation study.

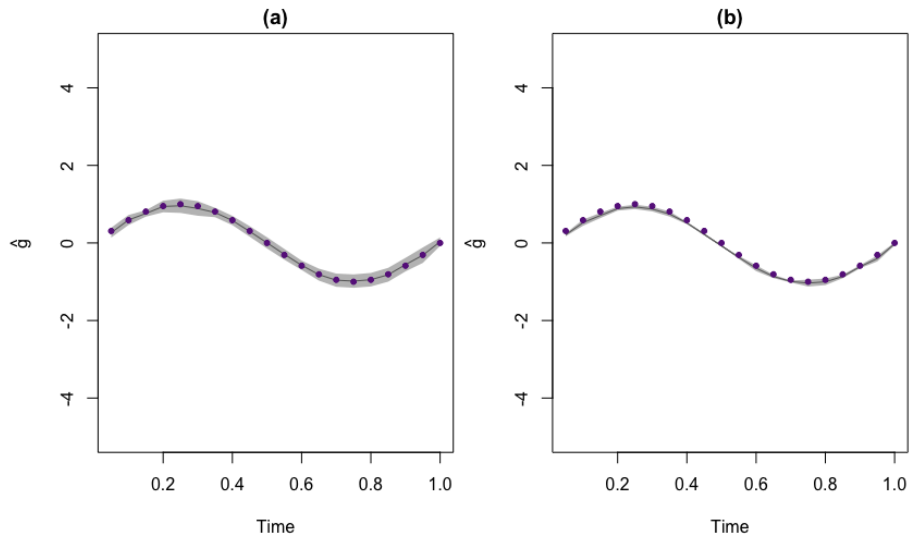


Figure 8: Plot of the estimated curve superimposed by its 95% CI for the B-spline for different values of  $n_k$ ,  $k = 1, \dots, K = 100$ . (a):  $n_k = 20$ , (b):  $n_k = 50$ .

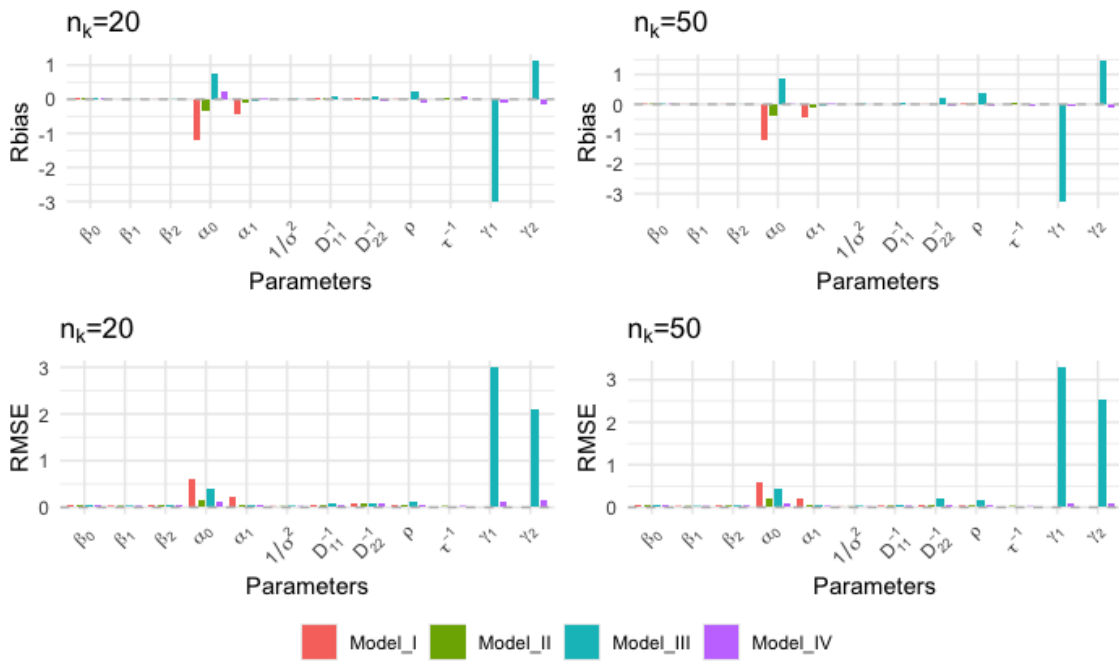


Figure 9: Comparison of Rbias and RMSE across four models (model I to model IV) in scenario 1 of the simulation study.

Table 3: Simulation Study Results for the Spatial Joint Model: Parameter Estimates, Standard Errors, Relative Bias, and RMSE for Scenario 1 with  $M=100$  Simulations and  $n_k = 20, 50$ .

$n_k$	Parameter	Model I						Model II						Model III						Model IV							
		Real	Est.	S.E.	Rbias	RMSE		Est.	S.E.	Rbias	RMSE		Est.	S.E.	Rbias	RMSE		Est.	S.E.	Rbias	RMSE		Est.	S.E.	Rbias	RMSE	
20	$\beta_0$	2.000	2.041	0.041	0.021	0.047		2.041	0.041	0.021	0.047		2.048	0.040	0.024	0.051		2.042	0.040	0.021	0.047		2.042	0.040	0.021	0.047	
	$\beta_1$	-1.000	-1.001	0.027	0.001	0.021		-1.001	0.027	0.001	0.021		-0.997	0.026	-0.003	0.021		-0.999	0.027	-0.001	0.021		-0.999	0.027	-0.001	0.021	
	$\beta_2$	1.000	0.996	0.056	-0.004	0.042		0.996	0.056	-0.004	0.042		0.993	0.054	-0.007	0.043		0.997	0.054	-0.003	0.042		0.997	0.054	-0.003	0.042	
	$\alpha_0$	0.500	-0.103	0.090	-1.206	0.603		0.336	0.054	-0.328	0.164		0.887	0.062	0.774	0.387		0.607	0.049	0.214	0.117		0.607	0.049	0.214	0.117	
	$\alpha_1$	-0.500	-0.290	0.039	-0.420	0.210		-0.443	0.040	-0.115	0.058		-0.461	0.049	-0.078	0.051		-0.486	0.038	-0.028	0.034		-0.486	0.038	-0.028	0.034	
	$1/\sigma^2$	1.000	0.999	0.012	-0.001	0.009		0.999	0.012	-0.001	0.009		0.981	0.011	-0.019	0.019		1.004	0.012	0.004	0.010		1.004	0.012	0.004	0.010	
	$D_{11}^{-1}$	1.000	1.015	0.048	0.015	0.041		1.016	0.048	0.016	0.041		1.073	0.050	0.073	0.075		1.007	0.046	0.007	0.038		1.007	0.046	0.007	0.038	
	$D_{22}^{-1}$	1.000	1.014	0.087	0.014	0.071		1.015	0.088	0.015	0.071		1.098	0.072	0.098	0.102		0.938	0.064	-0.062	0.071		0.938	0.064	-0.062	0.071	
	$\rho$	0.500	0.495	0.057	-0.011	0.043		0.494	0.057	-0.011	0.042		0.610	0.027	0.220	0.110		0.448	0.042	-0.104	0.056		0.448	0.042	-0.104	0.056	
	$\tau_{-1}$	0.100	-	-	-	-		0.105	0.018	0.049	0.014		-	-	-	-		0.093	0.015	-0.070	0.017		0.093	0.015	-0.070	0.017	
	$\gamma_1$	1.000	-	-	-	-		-	-	-	-		1.998	0.168	-2.998	2.998		0.887	0.059	-0.113	0.113		0.887	0.059	-0.113	0.113	
	$\gamma_2$	-1.000	-	-	-	-		-	-	-	-		-2.109	0.174	1.109	2.109		-0.834	0.056	-0.166	0.166		-0.834	0.056	-0.166	0.166	
	DIC							54138					51593					52383					50930				
	WAIC							54228					51778					54320					51258				
Computational time							0.100 (0.212)					0.134 (0.042)					0.205 (0.052)					0.448 (0.476)					
50	$\beta_0$	2.000	2.041	0.026	0.020	0.042		2.041	0.026	0.020	0.042		2.041	0.025	0.020	0.043		2.040	0.025	0.020	0.042		2.040	0.025	0.020	0.042	
	$\beta_1$	-1.000	-1.005	0.018	0.005	0.015		-1.005	0.018	0.005	0.015		-1.001	0.018	0.001	0.015		-1.002	0.018	0.002	0.015		-1.002	0.018	0.002	0.015	
	$\beta_2$	1.000	0.995	0.036	-0.005	0.029		0.995	0.036	-0.005	0.029		0.997	0.036	-0.003	0.029		0.996	0.036	-0.004	0.028		0.996	0.036	-0.004	0.028	
	$\alpha_0$	0.500	-0.100	0.083	-1.199	0.600		0.308	0.038	-0.383	0.192		0.923	0.056	0.846	0.423		0.507	0.040	0.014	0.097		0.507	0.040	0.014	0.097	
	$\alpha_1$	-0.500	-0.290	0.027	-0.420	0.210		-0.438	0.021	-0.125	0.062		-0.466	0.032	-0.068	0.038		-0.489	0.019	-0.022	0.018		-0.489	0.019	-0.022	0.018	
	$1/\sigma^2$	1.000	1.001	0.007	0.001	0.006		1.001	0.008	0.001	0.006		0.980	0.007	-0.020	0.020		1.002	0.007	0.002	0.006		1.002	0.007	0.002	0.006	
	$D_{11}^{-1}$	1.000	0.999	0.030	-0.001	0.024		1.000	0.032	0.000	0.026		1.073	0.040	0.073	0.073		0.996	0.029	-0.004	0.024		0.996	0.029	-0.004	0.024	
	$D_{22}^{-1}$	1.000	0.993	0.054	-0.007	0.046		0.995	0.053	-0.005	0.045		1.195	0.085	0.195	0.196		0.964	0.046	-0.036	0.047		0.964	0.046	-0.036	0.047	
	$\rho$	0.500	0.486	0.033	-0.028	0.028		0.489	0.036	-0.023	0.030		0.686	0.027	0.372	0.186		0.471	0.027	-0.058	0.034		0.471	0.027	-0.058	0.034	
	$\tau_{-1}$	0.100	-	-	-	-		0.108	0.020	0.075	0.016		-	-	-	-		0.095	0.016	-0.050	0.011		0.095	0.016	-0.050	0.011	
	$\gamma_1$	1.000	-	-	-	-		-	-	-	-		2.258	0.553	-3.258	3.292		0.919	0.036	-0.081	0.082		0.919	0.036	-0.081	0.082	
	$\gamma_2$	-1.000	-	-	-	-		-	-	-	-		-2.438	0.699	1.438	2.520		-0.891	0.041	-0.109	0.109		-0.891	0.041	-0.109	0.109	
	DIC							135283					130859					127908					127146				
	WAIC							134404					130254					127608					127146				
Computational time							0.250 (0.052)					0.425 (0.812)					0.640 (0.458)					0.803 (0.437)					

## 4.2 Scenario 2

In this scenario, we aim to replicate the data using real values similar to those obtained in the application section. For this purpose, we will utilize models (14) and (15), where Age is generated from a standard normal distribution, and both Gender and PrevOI are generated from a Bernoulli distribution with a success probability of 0.5. The same function as in the previous simulation study,  $g(t) = \sin(2\pi t)$ , will be used.

The parameters are defined as follows:  $\beta = (\beta_0, \beta_1, \beta_2, \beta_3)' = (9, -1, -1, -1.5)'$ ,  $\alpha = (\alpha_0, \alpha_1, \alpha_2, \alpha_3)' = (-6, 0.5, 0.5, 1)'$ ,  $\gamma_1 = -0.2$ ,  $\gamma_2 = -0.5$ , and  $\varpi = 2$ . The random effects are defined as  $\mathbf{b}_{ik} = (b_{0ik}, b_{1ik})' \sim N_2(\mathbf{0}, \mathbf{D}^{-1})$ , where

$$\mathbf{D} = \begin{pmatrix} 25 & -4 \\ -4 & 6 \end{pmatrix}$$

resulting in  $D_{11}^{-1} = 0.04$ ,  $D_{22}^{-1} = 0.167$ ,  $\rho = -0.326$ ,  $\sigma^2 = 5$ , and  $\tau = 12$ .

The results summarized in Table 4 and Figure 10 present the performance of four models in estimating parameters within a spatial joint model framework under Scenario 2, using  $M = 100$  simulations and a sample size of  $n_k = 50$ . Each model's estimates, standard errors (S.E.), relative bias (Rbias), and root mean squared error (RMSE) are reported for various parameters.

Model I (separate models without spatial effects) generally shows high relative biases and RMSEs for most parameters, particularly for  $\alpha_0$  and  $\varpi$ , indicating less reliable estimates. For example,  $\alpha_0$  is estimated at  $-3.584$  with a significant negative Rbias of  $-0.403$  and an RMSE of 2.416. Model II (separate models with spatial effects) improves upon Model I, with more accurate estimates, particularly for the spatial variance parameters  $D_{11}^{-1}$  and  $D_{22}^{-1}$ , which are estimated closer to their true values, although biases remain notable. Model III (joint model without spatial effects) exhibits better parameter estimates than Models I and II, with smaller Rbias and RMSE values across several parameters, including  $\beta_0$  and  $\beta_2$ . However, it still fails to fully leverage spatial correlations. Model IV (joint model with spatial effects) stands out as the most effective, yielding the closest estimates to the true values for most parameters, including  $\beta_0$  (est. 9.045, Rbias 0.005, RMSE 0.163) and  $\alpha_1$  (est. 0.478, Rbias  $-0.044$ , RMSE 0.089).

The DIC and WAIC values further confirm the superiority of Model IV, with DIC at 68136 and WAIC at 68281, both significantly lower than those of the other models. This suggests that Model IV provides a substantially better fit to the data.

Regarding computational efficiency, Model I has the shortest average computational time (mean 0.084 minutes), while Model IV takes longer (mean 0.422 minutes). Despite this increase, the time remains relatively low, indicating that the complexity of the model does not excessively hinder performance.

Overall, the findings suggest that incorporating spatial effects and employing a joint modeling approach significantly enhances parameter estimation accuracy. Model IV emerges as the best model, emphasizing the critical role of spatial correlations in analysis.

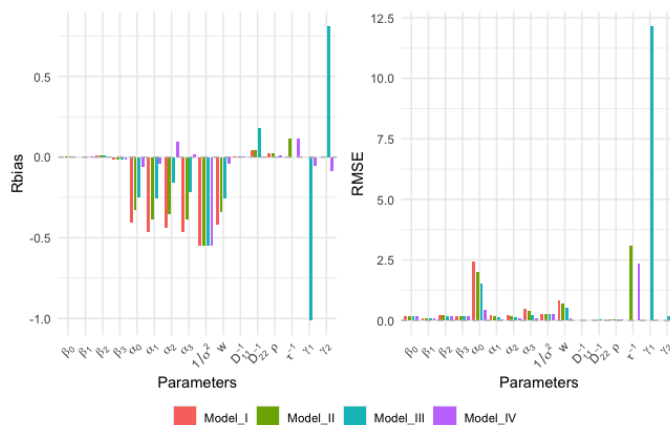


Figure 10: Comparison of Rbias and RMSE across four models (model I to model IV) in scenario 1 of the simulation study.



Table 4: Simulation Study Results for the Spatial Joint Model: Parameter Estimates, Standard Errors, Relative Bias, and RMSE for Scenario 2 with  $M=100$  Simulations and  $n_k = 50$ . The computational time is measured in minutes and includes the mean (standard deviation).

Parameter	Model I					Model II					Model III					Model IV					
	Real	Est.	S.E.	Rbias	RMSE	Est.	S.E.	Rbias	RMSE	Est.	S.E.	Rbias	RMSE	Est.	S.E.	Rbias	RMSE	Est.	S.E.	Rbias	RMSE
$\beta_0$	9.000	9.029	0.215	0.003	0.159	9.029	0.215	0.003	0.159	9.033	0.217	0.004	0.161	9.045	0.217	0.005	0.163	-1.003	0.130	0.003	0.103
$\beta_1$	-1.000	-0.999	0.129	-0.001	0.103	-0.999	0.129	-0.001	0.103	-1.001	0.130	0.001	0.103	-1.003	0.130	0.003	0.103	-1.006	0.246	0.006	0.197
$\beta_2$	-1.000	-1.012	0.246	0.012	0.198	-1.012	0.246	0.012	0.198	-1.009	0.246	0.009	0.197	-1.474	0.239	-0.017	0.192	-1.478	0.246	-0.017	0.192
$\beta_3$	-1.500	-1.478	0.239	-0.015	0.192	-1.478	0.239	-0.015	0.192	-4.478	0.762	-0.015	0.192	-4.485	0.762	-0.015	0.192	-4.478	0.762	-0.015	0.192
$\alpha_0$	-6.000	-3.584	0.380	-0.403	2.416	-4.021	0.149	-0.330	1.979	-4.485	0.762	-0.252	1.515	-5.627	0.332	-0.062	0.416	-5.627	0.332	-0.062	0.416
$\alpha_1$	0.500	0.267	0.046	-0.466	0.293	0.306	0.036	-0.387	0.194	0.372	0.082	-0.257	0.134	0.478	0.054	-0.044	0.044	0.478	0.054	-0.044	0.044
$\alpha_2$	0.500	0.281	0.073	-0.439	0.219	0.325	0.058	-0.351	0.175	0.422	0.121	-0.156	0.121	0.548	0.103	0.097	0.089	0.548	0.103	0.097	0.089
$\alpha_3$	1.000	0.535	0.075	-0.465	0.465	0.616	0.062	-0.384	0.384	0.781	0.155	-0.219	0.231	1.015	0.109	0.015	0.083	1.015	0.109	0.015	0.083
$1/\sigma^2$	0.447	0.200	0.003	-0.552	0.247	0.200	0.003	-0.552	0.247	0.201	0.003	-0.551	0.247	0.201	0.003	-0.550	0.246	0.201	0.003	-0.550	0.246
$\tau$	2.000	1.156	0.127	-0.422	0.844	1.321	0.045	-0.340	0.679	1.487	0.262	-0.257	0.513	1.920	0.101	-0.040	0.099	1.920	0.101	-0.040	0.099
$D_{11}^{-1}$	0.040	0.040	0.002	0.002	0.001	0.040	0.002	0.001	0.001	0.040	0.002	0.002	0.001	0.040	0.002	-0.002	0.001	0.040	0.002	-0.002	0.001
$D_{22}^{-1}$	0.167	0.174	0.015	0.045	0.012	0.174	0.015	0.045	0.012	0.196	0.226	0.179	0.039	0.166	0.015	-0.004	0.011	0.166	0.015	-0.004	0.011
$\rho$	-0.327	-0.334	0.037	0.023	0.031	-0.334	0.037	0.022	0.032	-0.326	0.078	-0.003	0.043	-0.330	0.039	0.010	0.033	-0.330	0.039	0.010	0.033
$\tau^{-1}$	12.000	-	-	-	-	13.414	3.157	0.118	3.087	-	-	-	-	13.399	2.532	0.116	2.336	-	-	-	-
$\gamma_1$	-0.200	-	-	-	-	-	-	-	-	-0.147	0.025	-1.012	12.147	-0.189	0.015	-0.054	0.015	-0.189	0.015	-0.054	0.015
DIC	-0.500	-	-	-	-	-	-	-	-	-0.362	0.075	0.810	0.162	-0.458	0.049	-0.084	0.052	-0.458	0.049	-0.084	0.052
WAC	-	-	-	-	-	-	-	-	-	-	-	-	-	-	-	-	-	-	-	-	-
Computational time	-	-	69401	-	-	-	-	68978	-	-	-	68806	-	-	-	68136	-	-	-	-	68281
	-	-	69485	-	-	-	-	69067	-	-	-	68919	-	-	-	68281	-	-	-	-	68281
	-	-	0.084 (0.012)	-	-	-	-	0.111 (0.020)	-	-	-	0.322 (0.075)	-	-	-	0.422 (0.159)	-	-	-	-	0.422 (0.159)

### 4.3 Scenario 3

The purpose of this scenario is to evaluate the performance and results of Model IV when implemented using two different Bayesian inference methods: Gibbs sampling through **R2OpenBUGS** and approximate Bayesian inference via **INLA**. Utilizing a consistent dataset (generated as in Scenario 2 with  $n_k = 20$ ), this comparison allows for an assessment of differences in estimation accuracy, computational efficiency, and overall feasibility between the two approaches. For the Gibbs sampler, we executed 10,000 iterations and assessed parameter convergence using the Gelman-Rubin criterion. The results, reported in Table 5 and illustrated in Figure 11, span 100 simulations and present parameter estimates, standard errors, relative bias, and RMSE for various parameters. Additionally, the table and figure highlight both the accuracy and variability of the estimates across the two methods. Notably, approximate Bayesian inference via **INLA** generally achieved closer estimates with lower computational demands, completing simulations in an average of 0.124 minutes compared to 339 minutes for Gibbs sampling. These results indicate that while both methods offer robust estimates, **INLA** demonstrates higher computational efficiency, making it potentially more feasible for large-scale or time-sensitive applications. The insights gained from this scenario provide valuable information on the trade-offs between Gibbs sampling and approximate Bayesian inference, particularly when balancing computational speed with estimation accuracy in spatial joint models.

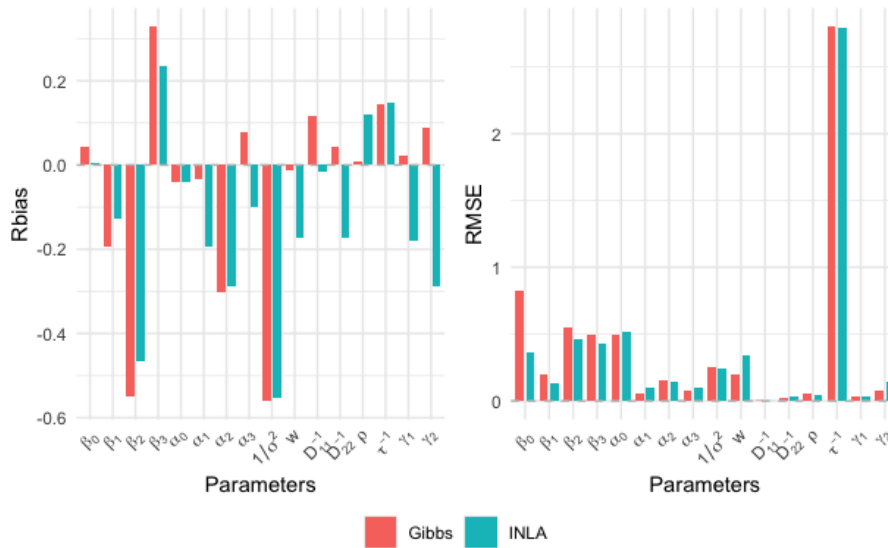


Figure 11: Comparison of Rbias and RMSE between Gibbs Sampling and Approximate Bayesian Inference (INLA) methods under Scenario 3 of the simulation study.

Table 5: Simulation Study Results for the Spatial Joint Model: Parameter Estimates, Standard Errors, Relative Bias, and RMSE for Scenario 3 with M=100 Simulations and  $n_k = 20$ . The computational time is measured in minutes and includes the mean (standard deviation).

Parameter	Real	Approximate Bayesian Inference				Gibbs Sampling			
		Est.	S.E.	Rbias	RMSE	Est.	S.E.	Rbias	RMSE
$\beta_0$	9.000	9.045	0.519	0.005	0.367	9.400	1.162	0.044	0.822
$\beta_1$	-1.000	-0.872	0.066	-0.128	0.128	-0.805	0.132	-0.195	0.195
$\beta_2$	-1.000	-0.534	0.520	-0.465	0.465	-0.449	0.504	-0.551	0.551
$\beta_3$	-1.500	-1.854	0.607	0.236	0.429	-1.994	0.507	0.329	0.494
$\alpha_0$	-6.000	-5.758	0.424	-0.040	0.519	-5.755	0.698	-0.041	0.494
$\alpha_1$	0.500	0.404	0.049	-0.193	0.096	0.483	0.074	-0.034	0.052
$\alpha_2$	0.500	0.356	0.178	-0.288	0.144	0.349	0.210	-0.303	0.151
$\alpha_3$	1.000	0.901	0.011	-0.099	0.099	1.078	0.038	0.078	0.078
$1/\sigma^2$	0.447	0.200	0.006	-0.552	0.247	0.197	0.001	-0.560	0.251
$\varpi$	2.000	1.654	0.136	-0.173	0.346	1.975	0.277	-0.012	0.196
$D_{11}^{-1}$	0.040	0.039	0.001	-0.017	0.001	0.045	0.001	0.118	0.005
$D_{22}^{-1}$	0.167	0.138	0.030	-0.172	0.029	0.174	0.039	0.044	0.027
$\rho$	-0.327	-0.365	0.050	0.119	0.039	-0.330	0.070	0.010	0.050
$\tau^{-1}$	12.000	13.791	2.885	0.149	2.789	13.731	2.901	0.144	2.803
$\gamma_1$	-0.200	-0.164	0.014	-0.181	0.036	-0.205	0.041	0.024	0.029
$\gamma_2$	-0.500	-0.355	0.058	-0.289	0.145	-0.545	0.113	0.089	0.080
Computational time		0.124 (0.075)				339 (12.543)			

#### 4.4 Key findings from simulation studies

In summary, the simulation study demonstrates that the proposed spatial joint model with spatial random effects (Model IV) consistently outperforms the other models across various parameter estimation metrics. Model IV effectively incorporates spatial correlations and jointly analyzes outcomes, resulting in significantly lower bias and RMSE values compared to separate models (Model I and II) and the joint model without spatial effects (Model III). The findings highlight the critical importance of considering spatial effects and employing a joint modeling approach for accurate parameter estimates. Additionally, larger sample sizes enhance estimation precision, underscoring the need for adequate data in spatial joint modeling contexts. Model IV is further validated by DIC and WAIC metrics, confirming its superior fit to the data and establishing it as the optimal choice for the analyzed scenarios.

## 5 Discussion

This paper presents an innovative approach to address the joint modeling of longitudinal measurements and spatial survival data, building upon the groundwork laid by [37] through the utilization of a Bayesian framework. While Bayesian methods offer powerful tools for inference in complex models, the computational demands associated with Markov Chain Monte Carlo (MCMC) algorithms can be prohibitive, especially in the context of joint modeling where multiple data sources are integrated. The computational complexity and time-consuming nature of MCMC hinder its scalability and practical application, particularly in large-scale studies or scenarios where timely analyses are imperative.

In response to these challenges, the study proposes an alternative methodology that leverages the Integrated Nested Laplace Approximation (INLA) technique. INLA provides a computationally efficient approximation method for Bayesian inference, offering considerable reductions in computation time compared to traditional MCMC approaches. By circumventing the need for lengthy MCMC iterations, INLA enables researchers to obtain accurate estimates and credible intervals in a fraction of the time, facilitating the rapid analysis of longitudinal and spatial data. This advancement is particularly significant in fields such as epidemiology and public health, where timely insights are crucial for informing policy and intervention strategies.

Furthermore, the methodology introduced in this paper addresses an important aspect of longitudinal data analysis—the nonlinear relationship between observed time and longitudinal responses. Traditional linear models may inadequately capture the complex temporal dynamics inherent in longitudinal data, leading to biased estimates and diminished model fit. By incorporating spline functions, the proposed approach offers a flexible framework capable of accommodating nonlinear trends in longitudinal responses. This enhancement not only improves the model’s predictive accuracy but also enhances its interpretability by capturing the nuanced relationships between time and outcome variables.

Overfitting occurs when a model becomes too complex, capturing both the true underlying patterns in the data and random noise, which results in poor generalization to unseen data [28]. In our paper, we

address this concern by employing several techniques that mitigate overfitting. First, our Bayesian hierarchical framework incorporates prior distributions that regularize the model, preventing it from becoming overly complex [24]. We also use penalized splines for modeling the non-linear time effects, where the optimal number of knots is selected based on generalized cross-validation to avoid unnecessary flexibility [17]. Furthermore, we model spatial dependencies using a GMRF, which includes precision matrices that regularize the spatial effects and reduce the risk of overfitting [50].

To assess and quantify overfitting, we apply model selection criteria such as the Deviance Information Criterion (DIC) and Watanabe-Akaike Information Criterion (WAIC), both of which penalize models based on their complexity and ensure a balance between goodness of fit and simplicity [54, 24]. Additionally, we evaluate relative bias (Rbias) and root of mean squared error (RMSE) in our simulation studies to ensure that our models are accurate and robust without overfitting. The consistency of these metrics across different simulations, including various sample sizes and model complexities, demonstrates that our approach effectively generalizes to unseen data without overfitting. The provision of R code for implementing the proposed spatial joint model enhances the accessibility and reproducibility of the research findings. The R code is available in <https://github.com/tbaghfalaki/ASJM>. Researchers can readily replicate the analyses conducted in the study, explore alternative modeling strategies, and adapt the methodology to suit diverse research contexts and datasets.

Looking forward, there are several promising avenues for extending the proposed framework. One potential direction involves the expansion of the model to accommodate multivariate longitudinal data or multivariate mixed longitudinal data, where multiple correlated outcomes are observed over time. By incorporating additional response variables, researchers can gain deeper insights into complex biological processes and disease trajectories, thereby enhancing the model's utility in clinical and epidemiological research.

Additionally, addressing the challenges associated with competing risks represents another important area of future investigation. Competing risks arise when individuals face multiple mutually exclusive events, such as death from different causes, and accounting for these complexities is essential for accurate risk estimation and decision-making. Developing robust methodologies for handling competing risks within the framework of joint modeling will further enhance the model's applicability in diverse research settings.

Furthermore, addressing missing data remains a critical area of ongoing research, particularly in longitudinal studies where dropout, intermittent non-response, or measurement error is common. Proper handling of missing data is crucial for ensuring unbiased inference and reliable results. By incorporating advanced imputation methods or adopting principled approaches such as multiple imputation, researchers can effectively mitigate the effects of missing data on model estimates. Specifically, for spatial data, the authors recommend leveraging the inherent spatial structure to impute missing values based on neighboring regions, as the Besag model assumes spatial dependence [7]. A simple approach involves imputing missing values using the mean of neighboring regions, while a more sophisticated option is model-based imputation using Bayesian inference, where missing values are estimated as part of the overall model through techniques such as MCMC [50]. Additionally, the proper Besag model with regularization can stabilize the imputation process by borrowing strength from observed data. To further account for uncertainty in missing data, multiple imputation techniques can be applied, combining results from multiple imputed datasets to enhance the robustness of findings [46].

This paper primarily focuses on right censoring of survival data. Although other types of censoring, such as interval or left censoring, are not explicitly addressed, the proposed model could potentially be extended to accommodate these mechanisms. Adapting the model for different types of censoring would likely necessitate some modifications; however, the general framework may still be applicable with the appropriate adjustments.

In summary, the methodology proposed in this paper represents a significant advancement in the field of joint modeling, offering a versatile and efficient framework for analyzing complex longitudinal and spatial data. By combining innovative computational techniques with sophisticated modeling strategies, this research opens new avenues for exploring the intricate relationships between longitudinal measurements and spatial survival outcomes, ultimately contributing to improved understanding and management of disease processes and public health challenges.

For future work, the proposed model could be extended to handle zero-inflated longitudinal outcomes [3], addressing scenarios where excess zeros occur alongside spatial dependencies for more comprehensive real-world applications.

## References

- [1] Maha Alesfri, Maria Sudell, Marta García-Fiñana, and Ruwanthi Kolamunnage-Dona. Bayesian joint modelling of longitudinal and time to event data: a methodological review. *BMC Medical Research Methodology*, 20(1):1–17, 2020.
- [2] Carmen Armero, Carles Forné, Montserrat Rué, Anabel Forte, Hèctor Perpiñán, Guadalupe Gómez, and Marisa Baré. Bayesian joint ordinal and survival modeling for breast cancer risk assessment. *Statistics in Medicine*, 35(28):5267–5282, 2016.
- [3] T Baghfalaki and M Ganjali. Approximate bayesian inference for joint linear and partially linear modeling of longitudinal zero-inflated count and time to event data. *Statistical Methods in Medical Research*, 30(6):1484–1501, 2021.
- [4] Taban Baghfalaki, Mojtaba Ganjali, and Damon Berridge. Joint modeling of multivariate longitudinal mixed measurements and time to event data using a bayesian approach. *Journal of Applied Statistics*, 41(9):1934–1955, 2014.
- [5] Taban Baghfalaki, Shiva Kalantari, Mojtaba Ganjali, Farzad Hadaegh, and Bagher Pahlavanzadeh. Bayesian joint modeling of ordinal longitudinal measurements and competing risks survival data for analysing tehran lipid and glucose study. *Journal of Biopharmaceutical Statistics*, 30(4):689–703, 2020.
- [6] M.A. Beaumont. Approximate bayesian computation in evolution and ecology. *Annual Review of Ecology, Evolution, and Systematics*, 41:379–406, 2010.
- [7] Julian Besag. Spatial interaction and the statistical analysis of lattice systems. *Journal of the Royal Statistical Society: Series B (Methodological)*, 36(2):192–225, 1974.
- [8] Julian Besag. Statistical analysis of non-lattice data. *Journal of the Royal Statistical Society: Series D (The Statistician)*, 24(3):179–195, 1975.
- [9] D.M. Blei, A. Kucukelbir, and J.D. McAuliffe. Variational inference: A review for statisticians. *Journal of the American Statistical Association*, 112(518):859–877, 2017.
- [10] D Brook. On the distinction between the conditional probability and the joint probability approaches in the specification of nearest-neighbour systems. *Biometrika*, 51(3/4):481–483, 1964.
- [11] Ming-Hui Chen, Joseph G Ibrahim, and Debajyoti Sinha. A new joint model for longitudinal and survival data with a cure fraction. *Journal of Multivariate Analysis*, 91(1):18–34, 2004.
- [12] Qingxia Chen, Ryan C May, Joseph G Ibrahim, Haitao Chu, and Stephen R Cole. Joint modeling of longitudinal and survival data with missing and left-censored time-varying covariates. *Statistics in Medicine*, 33(26):4560–4576, 2014.
- [13] Nicholas C Chesnaye, Giovanni Tripepi, Friedo W Dekker, Carmine Zoccali, Aeilko H Zwinderman, and Kitty J Jager. An introduction to joint models—applications in nephrology. *Clinical Kidney Journal*, 13(2):143–149, 2020.
- [14] Yueh-Yun Chi and Joseph G Ibrahim. Joint models for multivariate longitudinal and multivariate survival data. *Biometrics*, 62(2):432–445, 2006.
- [15] David R Cox and E Joyce Snell. A general definition of residuals. *Journal of the Royal Statistical Society: Series B (Methodological)*, 30(2):248–265, 1968.
- [16] Dennis Deapen, Myles Cockburn, Rich Pinder, Sharon Lu, and Amy Rock Wohl. Population-based linkage of aids and cancer registries: importance of linkage algorithm. *American journal of American Journal of Preventive Medicine medicine*, 33(2):134–136, 2007.
- [17] Paul HC Eilers and Brian D Marx. Flexible smoothing with b-splines and penalties. *Statistical Science*, 11(2):89–121, 1996.
- [18] Robert Elashoff, Ning Li, et al. *Joint Modeling of Longitudinal and Time-to-Event Data*. CRC Press, Boca Raton, FL, 2016.
- [19] Maria Goretti Pereira Fonseca, Cláudia Medina Coeli, Francisca de Fátima de Araújo Lucena, Valdilea Gonçalves Veloso, and Marília Sá Carvalho. Accuracy of a probabilistic record linkage strategy applied to identify deaths among cases reported to the brazilian aids surveillance database. *Cadernos de saúde pública*, 26:1431–1438, 2010.
- [20] Allison KC Furgal, Ananda Sen, and Jeremy MG Taylor. Review and comparison of computational approaches for joint longitudinal and time-to-event models. *International Statistical Review*, 87(2):393–418, 2019.
- [21] M Ganjali and T Baghfalaki. A copula approach to joint modeling of longitudinal measurements and survival times using monte carlo expectation-maximization with application to aids studies. *Journal of biopharmaceutical statistics*, 25(5):1077–1099, 2015.
- [22] Gebru Gebrerufael, Zeytu Asfaw, and Dessie Melese. Statistical joint modeling on longitudinal body weight and cd4 cell progression with survival time-to-death predictors on hiv/aids patients in mekelle general hospital, ethiopia. *Medicine*, 2020.
- [23] A. Gelman, J. Hwang, and A. Vehtari. Understanding predictive information criteria for bayesian models. *Statistics and Computing*, 24:997–1016, 2014.

- [24] Andrew Gelman, John B. Carlin, Hal S. Stern, David B. Dunson, Aki Vehtari, and Donald B. Rubin. *Bayesian Data Analysis*. CRC Press, Boca Raton, FL, 3rd edition, 2014.
- [25] W.R. Gilks, S. Richardson, and D.J. Spiegelhalter. *Markov Chain Monte Carlo in Practice*. Chapman and Hall/CRC, Boca Raton, FL, 1995.
- [26] Xu Guo and Bradley P Carlin. Separate and joint modeling of longitudinal and event time data using standard computer packages. *The american statistician*, 58(1):16–24, 2004.
- [27] Il Do Ha, Maengseok Noh, and Youngjo Lee. H-likelihood approach for joint modeling of longitudinal outcomes and time-to-event data. *Biometrical Journal*, 59(6):1122–1143, 2017.
- [28] Trevor Hastie, Robert Tibshirani, and Jerome Friedman. *The Elements of Statistical Learning: Data Mining, Inference, and Prediction*. Springer Science & Business Media, New York, NY, 2009.
- [29] Bo He and Sheng Luo. Joint modeling of multivariate longitudinal measurements and survival data with applications to parkinson’s disease. *Statistical Methods in Medical Research*, 25(4):1346–1358, 2016.
- [30] Graeme L Hickey, Pete Philipson, Andrea Jorgensen, and Ruwanthi Kolumunnage-Dona. Joint models of longitudinal and time-to-event data with more than one event time outcome: a review. *The International Journal of Biostatistics*, 14(1), 2018.
- [31] Fushing Hsieh, Yi-Kuan Tseng, and Jane-Ling Wang. Joint modeling of survival and longitudinal data: likelihood approach revisited. *Biometrics*, 62(4):1037–1043, 2006.
- [32] Kai Kang, Deng Pan, and Xinyuan Song. A joint model for multivariate longitudinal and survival data to discover the conversion to alzheimer’s disease. *Statistics in Medicine*, 41(2):356–373, 2022.
- [33] Catherine Legrand. *Advanced Survival Models*. Chapman and Hall/CRC, Boca Raton, FL, 2021.
- [34] Ning Li, Robert M Elashoff, Gang Li, and Jeffrey Saver. Joint modeling of longitudinal ordinal data and competing risks survival times and analysis of the ninds rt-pa stroke trial. *Statistics in Medicine*, 29(5):546–557, 2010.
- [35] Hugo Loureiro, Eunice Carrasquinha, Irina Alho, Arlindo R Ferreira, Luís Costa, Alexandra M Carvalho, and Susana Vinga. Modelling cancer outcomes of bone metastatic patients: combining survival data with n-telopeptide of type i collagen (ntx) dynamics through joint models. *BMC Medical Informatics and Decision Making*, 19(1):1–12, 2019.
- [36] Sheng Luo. A bayesian approach to joint analysis of multivariate longitudinal data and parametric accelerated failure time. *Statistics in Medicine*, 33(4):580–594, 2014.
- [37] Rui Martins, Giovanni L Silva, and Valeska Andreozzi. Bayesian joint modeling of longitudinal and spatial survival aids data. *Statistics in Medicine*, 35(19):3368–3384, 2016.
- [38] Rui Martins, Giovanni L Silva, and Valeska Andreozzi. Joint analysis of longitudinal and survival aids data with a spatial fraction of long-term survivors: A bayesian approach. *Biometrical Journal*, 59(6):1166–1183, 2017.
- [39] P Mehdizadeh, Taban Baghfalaki, M Esmailian, and M Ganjali. A two-stage approach for joint modeling of longitudinal measurements and competing risks data. *Journal of Biopharmaceutical Statistics*, 31(4):448–468, 2021.
- [40] Somayeh Momenyan. Joint analysis of longitudinal measurements and spatially clustered competing risks hiv/aids data. *Statistics in Medicine*, 40(28):6459–6477, 2021.
- [41] James Murray and Pete Philipson. A fast approximate em algorithm for joint models of survival and multivariate longitudinal data. *Computational Statistics & Data Analysis*, 170:107438, 2022.
- [42] Janet van Niekerk, Haakon Bakka, and Håvard Rue. Competing risks joint models using r-inla. *Statistical Modelling*, 21(1-2):56–71, 2021.
- [43] Grigorios Papageorgiou, Katya Mauff, Anirudh Tomer, and Dimitris Rizopoulos. An overview of joint modeling of time-to-event and longitudinal outcomes. *Annual Review of Statistics and Its Application*, 6:223–240, 2019.
- [44] Dimitris Rizopoulos. *Joint Models for Longitudinal and Time-to-Event Data: With Applications in R*. CRC Press, Boca Raton, FL, 2012.
- [45] Dimitris Rizopoulos and Pulak Ghosh. A bayesian semiparametric multivariate joint model for multiple longitudinal outcomes and a time-to-event. *Statistics in Medicine*, 30(12):1366–1380, 2011.
- [46] Donald B Rubin. *Multiple Imputation for Nonresponse in Surveys*. John Wiley & Sons, New York, NY, 1987.
- [47] H. Rue, S. Martino, and N. Chopin. Approximate bayesian inference for latent gaussian models by using integrated nested laplace approximations. *Journal of the Royal Statistical Society: Series B (Statistical Methodology)*, 71(2):319–392, 2009.
- [48] H. Rue, A. Riebler, S.H. Sørbye, J.B. Illian, D.P. Simpson, and F.K. Lindgren. Bayesian computing with inla: A review. *Annual Review of Statistics and Its Application*, 4:395–421, 2017.
- [49] Håvard Rue and Leonhard Held. *Gaussian Markov random fields: theory and applications*. Chapman and Hall/CRC, Boca Raton, FL, 2005.
- [50] Håvard Rue, Sara Martino, and Nicolas Chopin. Approximate bayesian inference for latent gaussian models by using integrated nested laplace approximations. *Journal of the Royal Statistical Society: Series B (Statistical Methodology)*, 71(2):319–392, 2009.

- [51] Denis Rustand, Janet Van Niekerk, Elias Teixeira Krainski, Håvard Rue, and Cécile Proust-Lima. Fast and flexible inference for joint models of multivariate longitudinal and survival data using integrated nested laplace approximations. *Biostatistics*, 25(2):429–448, 2024.
- [52] S.A. Sisson, Y. Fan, and M. Beaumont. *Handbook of Approximate Bayesian Computation*. CRC Press, Boca Raton, FL, 2018.
- [53] Inês Sousa. A review on joint modelling of longitudinal measurements and time-to-event. *REVSTAT-Statistical Journal*, 9(1):57–81, 2011.
- [54] David J Spiegelhalter, Nicky G Best, Bradley P Carlin, and Angelika van der Linde. Bayesian measures of model complexity and fit. *Journal of the Royal Statistical Society: Series B (Statistical Methodology)*, 64(4):583–639, 2002.
- [55] Laetitia Teixeira, Inês Sousa, Anabela Rodrigues, and Denisa Mendonça. Joint modelling of longitudinal and competing risks data in clinical research. *REVSTAT – Statistical Journal*, 2019.
- [56] Aboma Temesgen, Abdisa Gurmesa, and Yeheneu Getchew. Joint modeling of longitudinal cd4 count and time-to-death of hiv/tb co-infected patients: A case of jimma university specialized hospital. *Annals of Data Science*, 5(4):659–678, 2018.
- [57] Bsrat Tesfay, Tewodros Getinet, and Endeshaw Assefa Derso. Joint modeling of longitudinal change in tumor cell level and time to death of breast cancer patients: In case of ayder comprehensive specialized hospital tigray, ethiopia. *Cogent Medicine*, 8(1):1874090, 2021.
- [58] Janet Van Niekerk, Haakon Bakka, Håvard Rue, and Olaf Schenk. New frontiers in bayesian modeling using the inla package in r. *arXiv preprint arXiv:1907.10426*, 2019.
- [59] Xiaofeng Wang, Yuryan Yue, and Julian J Faraway. *Bayesian Regression Modeling with INLA*. Chapman and Hall/CRC, Boca Raton, FL, 2018.
- [60] Paula R Williamson, Ruwanthi Kolamunnage-Dona, Pete Philipson, and Anthony G Marson. Joint modelling of longitudinal and competing risks data. *Statistics in Medicine*, 27(30):6426–6438, 2008.
- [61] Hulin Wu and Jin-Ting Zhang. *Nonparametric Regression Methods for Longitudinal Data Analysis: Mixed-Effects Modeling Approaches*. John Wiley & Sons, Hoboken, NJ, 2006.
- [62] Lang Wu. *Mixed Effects Models for Complex Data*. Chapman and Hall/CRC, Boca Raton, FL, 2009.
- [63] Lu Yang, Hui Song, Yingwei Peng, and Dongsheng Tu. Joint analysis of longitudinal measurements and survival times with a cure fraction based on partly linear mixed and semiparametric cure models. *Pharmaceutical Statistics*, 20(2):362–374, 2021.
- [64] Huirong Zhu, Stacia M DeSantis, and Sheng Luo. Joint modeling of longitudinal zero-inflated count and time-to-event data: A bayesian perspective. *Statistical Methods in Medical Research*, 27(4):1258–1270, 2018.